Short-term Offshore Wind Speed Forecast by Seasonal ARIMA - A Comparison against GRU and LSTM

Xiaolei Liu[a], Zi Lin[b1], Ziming Feng[c]

[a] *James Watt School of Engineering, University of Glasgow, Glasgow, G12 8QQ, UK*
[b] *Department of Mechanical & Construction Engineering, Northumbria University, Newcastle upon Tyne, NE1 8ST, UK*
[c] *School of Mechanical Science and Engineering, Northeast Petroleum University, Heilongjiang, Daqing, 163318, China*

Abstract

Offshore wind power is one of the fastest-growing energy sources worldwide, which is environmentally friendly and economically competitive. Short-term time series wind speed forecasts are extremely significant for proper and efficient offshore wind energy evaluation and in turn, benefit wind farm owner, grid operators as well as end customers. In this study, a Seasonal Auto-Regression Integrated Moving Average (SARIMA) model is proposed to predict hourly-measured wind speeds in the coastal/offshore area of Scotland. The used datasets consist of three wind speed time series collected at different elevations from a coastal met mast, which was designed to serve for a demonstration offshore wind turbine. To verify SARIMA's performance, the developed predictive model was further compared with the newly developed deep-learning-based algorithms of Gated Recurrent Unit (GRU) and Long Short-Term Memory (LSTM). Regardless of the recent development of computational power has triggered more advanced machine learning algorithms, the proposed SARIMA model has shown its outperformance in the accuracy of forecasting future lags of offshore wind speeds along with time series. The SARIMA model provided the highest accuracy and robust healthiness among all the three tested predictive models based on corresponding datasets and assessed forecasting horizons.

Keywords: Wind speed forecasting; Seasonal Auto-Regression Integrated Moving Average (SARIMA); Deep learning; Long Short Term Memory (LSTM); Gated Recurrent Unit (GRU).

Nomenclature:

Latin symbols

$\tilde{h}_t$	Output candidate of the cell state vector
h_t	Cell state vector for time step t
h_{t-1}	Cell state vector for time step $t-1$

[1] Corresponding author, E-mail: zi.lin@northumbria.ac.uk (ZL)

Z_t	Observation at time t
f_t	Update gate
r_t	Reset gate
x_t	Input of neuron at time step t
D	Degree of seasonal differencing
L	Lag distance operator
P	Number of seasonal lag observations
Q	Order of seasonal moving average
U	Assigned weights
W	Assigned weights
b	Bias
c	Intercept term
d	Number of times that raw observations are differenced
i	represents how many terms in the time series are taken back from the current time t
n	Number of time steps
p	Number of lag observations
q	Size of moving average window
s	Length of the seasonal period
$(X_{forecasting})_t$	Predicted wind speed at time step t
$(X_{recorded})_t$	Recorded wind speed at time step t

Greek symbols

ϵ_t	Error term
∇	Differencing operator
B	Seasonal AR parameters
Θ	Seasonal MA parameters
β	Coefficient of lags
θ	Constant parameters

σ	Activation function

ABBREVIATION:

Adam	Adaptive moment estimation
ANN	Artificial Neural Network
AR	Autoregression
ARIMA	AutoRegressive Integrated Moving Average
ELM	Extreme Learning Machine
EVS	Explained Variance Score
GRNNs	Gated Recurrent Neural Networks
KDE	Kernel Density Estimation
KF	Kalman Filter
LSSVM	Least Square Support Vector Machine
LSTM	Long Short-Term Memory
MA	Moving Average
MAE	Mean Absolute Error
MedAE	Median Absolute Error
MSE	Mean Squared Error
O&M	Ooperation & Mmaintenance
R^2	R-square
RMSE	Root Mean Square Error
RNNs	Recurrent Neural Networks
RVFL	Random Vector Functional Link
SARIMA	Seasonal AutoRegressive Integrated Moving Average
SCADA	Supervisory Control And Data Acquisition
SVM	Support Vector Machine

1. Introduction

To meet the decarbonisation aim in 2050, the offshore wind industry is expected to experience a considerable increase in the coming several decades [1]. On this account, a large amount of new offshore wind farms will be designed, installed and monitored. The movements of offshore wind have the nature of randomness and are highly dependent on terrain and heights

[2]. Wind profile in the offshore sites are smoother and the loading of offshore turbines [3] are often larger than the onshore ones. Therefore, conventional methods designed for onshore wind speed prediction need to be re-developed for offshore wind forecasting.

Wind speed prediction is not only crucial for the design and installation of large wind farms but also essential for maintaining reliability and safe operation of the power network [4]. More specifically, short-term and extra short-term wind speed prediction [5] are becoming more and more popular through different prediction methods. However, investigation of offshore wind speed prediction remains under-represented Fig. 1 summarised recent investigations regarding wind speed forecasting since 2015, where the term of "onshore" is defined as locations in an in-land area, while "offshore" refers to areas situated at a certain distance from the shore. Besides, the term "nearshore" or "coastal" identifies the data collected from weather stations or wind farms that are in the coastal area or very close to the shoreline. Those wind speed data share common features as the offshore ones and are classified into the "offshore" category. As can be seen in Fig. 1, the majority of wind speed forecasting studies are onshore with very few case studies focused on offshore or nearshore areas.

Year of publications regarding wind speed forecasting	Onshore	Offshore
2015 [6–10]	5	-
2016 [11–18]	8	-
2017 [19–25]	7	1
2018 [26–31]	5	1
2019 [4,32,33]	2	1
2020 [34–36]	3	1

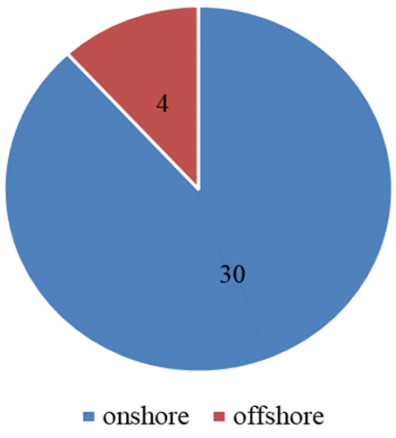

Fig. 1 – Summary of wind speed forecasting studies at different locations or areas since 2015 (note that wind speeds recorded from nearshore and coastal area were classified into the "offshore" category).

Wind speed prediction can be categorized on the basis of time horizons, as presented in Table 1. Note that, the forecasting accuracy is decreasing with the growth of prediction horizons. The current study will focus on the investigation of short-term offshore wind speed forecast, whose major applications cover economic load dispatch planning, reasonable decisions of load and operational security of maintaining wind turbines. Today, even countries with the most advance renewable energy sectors, such as the UK and Germany, are still confronting challenges in entirely depending on renewable sources. Grid operators have to turn to traditional power stations under unappreciated meteorological conditions to escape from overloading grid systems or power wasting, which may cause significant failures and noteworthy expenses. For example, in 2016 alone, around €454

million were taken from German consumers to cover the costs of compensating utility firms for tunings to their inputs [37]. Using available historical met mast data to predict short-term wind speed in advance of actual power generation could be one of the solutions [5].

Table 1 – Wind speed forecasting based on prediction horizons [38].

Time scales	*Time horizons*
Very short-term	< 8 hours
Short-term	⩽ 24 hours
Long-term	> 24 hours

In terms of analysis methods, wind speed prediction can also be divided into persistence, physical, statistical, and hybrid approaches [4]. Among these methods, the statistical method is often considered as the most suitable one for short-term forecasting [27]. Based on this approach, many researchers have focused on refining the accuracy of wind speed forecasting. For example, Kavasseri and Seetharaman [39] applied the fractional-ARIMA (Auto-Regression Integrated Moving Average) for predicting wind speed in both one-day and two-day time horizons. A case study, using a 750 kW wind turbine as the target, proved the advantage of the proposed model in terms of error reductions over a persistence model. Singh and Mohapatra [4] introduced a novel statistical model that outperformed the individual ARIMA forecasting, which was featured by combining repeated wavelet transform and ARIMA. Wang *et al.* [27] integrated the extreme learning model with ARIMA to predict short-term wind speeds. The predictive accuracy was proved through case studies using wind speed data measured from three different field sites. Cadenas and Rivera [40] presented a hybrid model to incorporate ARIMA and ANN (artificial neural network). The comparison results indicated that the developed combined model has higher accuracy than individual ones. Additionally, a novel ARIMA-based method was proposed by Shukur and Lee [41] to improve the accuracy and handle the uncertainties in wind speed forecasting. A more sophisticated model was proposed by Wang and Hu [42], which coupled ARIMA, Least Square Support Vector Machine (LSSVM), Support Vector Machine (SVM), and Extreme Learning Machine (ELM). Case studies, based on two wind farm datasets from China, showed that forecasted wind speeds were more accurate and more reliable compared with the predicted results by individual methods. Eymen et al [43] introduced a study of seasonal trend analysis of relative humidity and wind speed time series around a dam, where the post-dam relative humidity was forecasted by ARIMA models.

All above-mentioned predictive models are based on ARIMA, which can only perform well on stationary time series. However, time-series, like offshore wind speeds, have features of seasonality and trend. Those features become more prominent in offshore cases. This type of time series can be addressed by Seasonal-ARIMA (SARIMA), which has been widely applied in several different forecasting issues. For instance, Fang and Lahdelma [44] developed a SARIMA model to predict heat

demand in district heating systems. It claimed that the designed model provided a high accuracy for heat demand forecasting. Kushwaha and Pindoriya [45] presented a SARIMA-RVFL (Random Vector Functional Link) model to predict very short-term solar PV power generation, where a relatively high accuracy was achieved. However, in terms of wind speed forecasting, fewer researches focused on developing a SARIMA-based model, even though offshore wind speed varies seasonally. A simple and efficient SARIMA-based model was developed by Guo *et al.* [46], where the proposed method has improved accuracy over ARIMA-based methods for monthly wind speed prediction.

Offshore wind speeds are stochastic and uncertain, making accurate predictions a challenging task. However, offshore wind speed time series follow a seasonal periodical distribution, unlike the data used in other sectors. Therefore, using the SARIMA model for offshore wind speed prediction could offer better data consistency and potentially saving computational costs and enhancing forecasting accuracies. Few existing studies for short-term offshore wind speed prediction focus on using SARIMA-based approach. This paper will bridge above knowledge gaps by investigating short-term offshore wind speed forecasting through integrated SARIMA modelling.

Besides, in recent years, machine learning approaches [47], such as deep-learning-based LSTM and GRU [48], have been increasingly popular in wind energy forecasting. However, the conventional neural network method may cause overfitting in the training process, which make the forecasted result unrealistic. To this end, this paper also evaluated the accuracy of LSTM and GRU, which are recently developed machine learning algorithms, against the proposed SARIMA-based predictive models using data from a met mast that was designed for serving an offshore wind turbine [49]. This was realized in several phases defined by the adopted methodology, which involved visualizing offshore wind speed time series, identifying correlations, tuning hyperparameters through grid search and evaluating residual errors. The applied methodology of this study and the used time series predictive algorithm processing flowchart is summarised in Fig. 2 and Fig. 3, respectively.

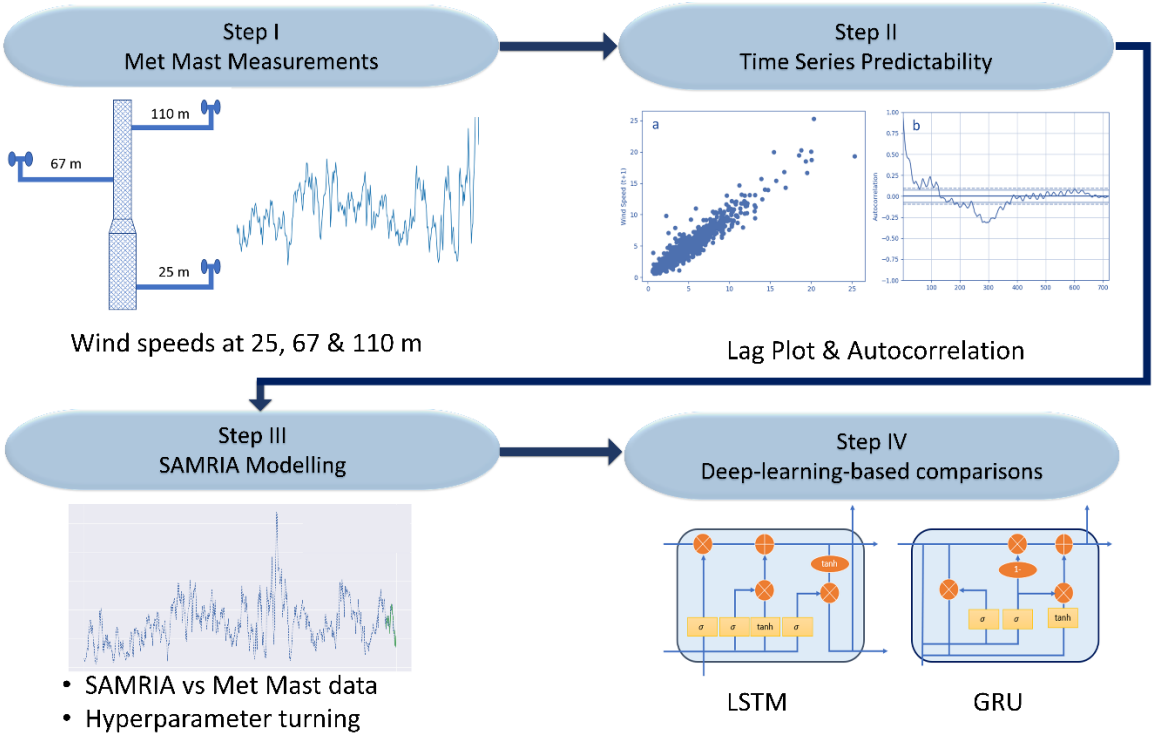

Fig. 2 – Diagram of applied methodology.

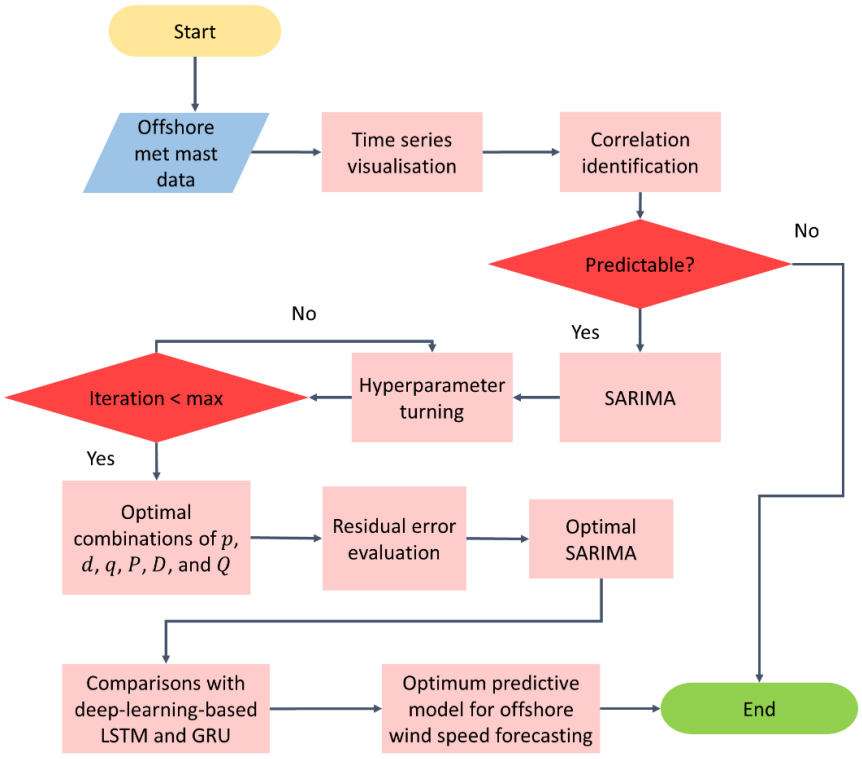

Fig. 3 – Offshore wind speed time series predictive algorithm processing flowchart.

The key contributions of this study to the current knowledge gaps of offshore wind speed forecasting can be summarized as follows:

- Propose an integrated forecasting method for short-term offshore wind speed predictions;
- Introduce the seasonal term to short-term offshore wind speed predictions through seasonal-ARIMA model;
- Validate the reliability of the proposed seasonal-ARIMA model with recently developed machine learning algorithms of LSTM and GRU.

The remainder of this paper is organized as follows. Section 2 described the used offshore wind speed time series databank, including how the met mast measurements were recorded. Section 3 depicted the methodologies behind the SARIMA. Then, the SARIMA predictive model was developed and validated for offshore short-term wind speed forecasting in section 4. The predictive results obtained from the designed SARIMA model were further compared with GRU and LSTM neural networks in section 5. Section 6 concludes this study by summarizing key findings and contributions of this paper.

2. Time series data description

The used offshore wind speed SCADA (Supervisory Control And Data Acquisition) database was collected from 01.01.2018 ~ 31.12.2018 by a measuring tower, which was designed to serve for a 7 MW demonstration offshore wind turbine situated in the coastal area of Scotland [50]. The met mast provided accurate offshore wind conditions for the turbine's operation & maintenance (O&M). It consists of 11 meteorological sensors installed at different heights, which can measure wind speeds (recorded by anemometers), wind directions (recorded by weathervanes), air pressure (recorded by barometers), and air temperature (recorded by thermometers). In this investigation, the extracted time-series database contains three historical wind speeds under a sampling rate of 1 Hz, which were collected at the height of 25 m, 67 m, and 110 m, respectively. The wind speed dataset was then resampled with a time interval of 1 h and was further used in the proposed time forecasting models.

3. Methodology

SARIMA, which is a variation of ARIMA, can support time-series predictions of univariate data containing trends and seasonality. It could control the seasonality of time series by including them as a feature in predictive models and explicitly cater to a set of classic structures in short-term datasets. SARIMA is short for Seasonal Auto-Regression Integrated Moving Average that is a seasonal expression of Auto-Regression and Moving Average while inserting the concept of Integration. Each of those components can be explicitly specified in SARIMA as an input number (feature), in which a classic notation of SARIMA (p, d, q) $(P, D, Q)_s$ is frequently applied. The input features of p, d, q, P, D , Q, and s stand with integer values, where p is the number of lag observations involved in the SARIMA model; d is the number of times that raw observations are differenced, also named as the degree of differencing; q is the size of the moving average window, also called as the order of moving average; P is the number of involved seasonal lag observations; D is the degree of seasonal differencing; Q is the order

of seasonal moving average, and the subscripted letter of s is often used to represent the length of the seasonal period, respectively. In time-series datasets, seasonal patterns can be circularly observed after a certain number of periodical values. For instance, the value of s can be set as 12 for monthly observations because one year has 12 months; for hourly observations, the value of s is often defined by 24 as one day has 24 hours. In summary, the major components in the SARIMA model are:

- Auto-Regression (AR) adopts the dependency between an observed value and previous lagged observed values for predictions. In wind speed forecasting, it would be similar to expressing that it is likely to be windy in the next hour if it has been windy in the past a few hours. In an individual AR model, the observation (Z_t) at time t only depends on its lags, which can be expressed as [51]:

$$Z_t = \beta_1 Z_{t-1} + \beta_2 Z_{t-2} + \cdots + \beta_p Z_{t-p} + \epsilon_t = \left(\sum_{i=1}^{p} \beta_i L^i\right) Z_t + \epsilon_t \quad (1)$$

  where $t = p+1, \ldots, n$; Z_t is the observation at time t; β is the coefficient of lags that the model estimates; ϵ_t is the error term; L is the lag distance operator; i represents how many terms are looked back from the current time t in the investigated time series.

- Moving Average (MA) uses correlations between an observation and the corresponding residual error from the moving average model that was applied to lagged observations. This component offers the opportunity to set the error in the model as a linear combination of residual errors observed at previous time steps. In an individual MA model, Z_t only depends on the lagged forecast errors, which can be stated as:

$$Z_t = \epsilon_t - \theta_1 \epsilon_{t-1} - \theta_2 \epsilon_{t-2} - \cdots - \theta_q \epsilon_{t-q} = \left(1 - \sum_{i=1}^{q} \theta_i L^i\right) \epsilon_t \quad (2)$$

  where $t = q+1, \ldots, n$; θ is the constant parameters that the model estimates; L is the lag distance operator; i represents how many terms in the time series are taken back from the current time t; the error terms ϵ are the inaccuracies of AR models of respective lags. For instance, ϵ_t and ϵ_{t-1} are the errors from the following expressions:

$$Z_t = \beta_1 Z_{t-1} + \beta_2 Z_{t-2} + \cdots + \beta_0 Z_0 + \epsilon_t \quad (3)$$

$$Z_{t-1} = \beta_1 Z_{t-2} + \beta_2 Z_{t-3} + \cdots + \beta_0 Z_0 + \epsilon_{t-1} \quad (4)$$

- Integrated (I) differences raw observations to smoothen the entire time series. In this study, it would be comparable to expressing that it is likely to be the same regime of winds in the next hour if the difference in wind regime in the last a few hours is very limited. Under more complicated circumstances, the models of AR and MA can be combined and the individual ARIMA expression can be summarized as:

$$\left(1-\sum_{i=1}^{p}\beta_i L^i\right)(1-L)^d Z_t = \left(1-\sum_{i=1}^{q}\theta_i L^i\right)\epsilon_t + c \tag{5}$$

If $\nabla = 1 - L$ is defined as the differencing operator, the Eq. (5) above can be further simplified as:

$$\beta_p(L)\nabla^d Z_t = \theta_q(L)\epsilon_t + c \tag{6}$$

where $t = \max(p+1, q+1), \ldots, n$; c is the intercept term.

Extended from Eq. (6), the general form of SARIMA expression can be stated as:

$$\beta_p(L)\mathrm{B}_P(L^s)\nabla^d\nabla_s^D Z_t = \theta_q(L)\Theta_Q(L^s)\epsilon_t + c \tag{7}$$

where B and β are seasonal and non-seasonal AR parameters, respectively; Θ and θ are seasonal and non-seasonal MA parameters, respectively; L is differencing operators.

4. SARIMA modelling

In this study, the standardized approach of Box-Jenkins methodology [52] was followed while developing the SARIMA model, which uses iterative diagnostics to unearth optimized hyperparameters in time series forecasting. It consists of three main steps:

- Model identification: evaluate trends, seasonality, and autoregression in the targeted wind speed time series by statistical analysis (see section 4.1 and 4.2);
- Parameter estimation: adjust hyperparameters to optimize the predictive model (see section 4.3);
- Model checking: identify residual errors from the modelling results to assess the temporal structure that cannot be captured by the current model (see section 4.4).

4.1 Time series analysis

Analysis and visualization of time series data could offer valuable diagnostics to define wind speeds' temporal structures of trend and seasonality. The variations of wind speeds and its distributions over September 2018 (one-month span) are plotted in Fig. 4a and b, respectively. In Fig. 4a, time intervals are presented on the x-axis with wind speed observations along the y-axis, where a baseline of wind variations is observed (see the dashed line in Fig. 4a). In Fig. 4b, the distribution of wind speed observations is summarised through box plots, where the medians of values were captured by drawn lines at the middle of boxes and very few dots were observed as outliers outside the extents of the current dataset.

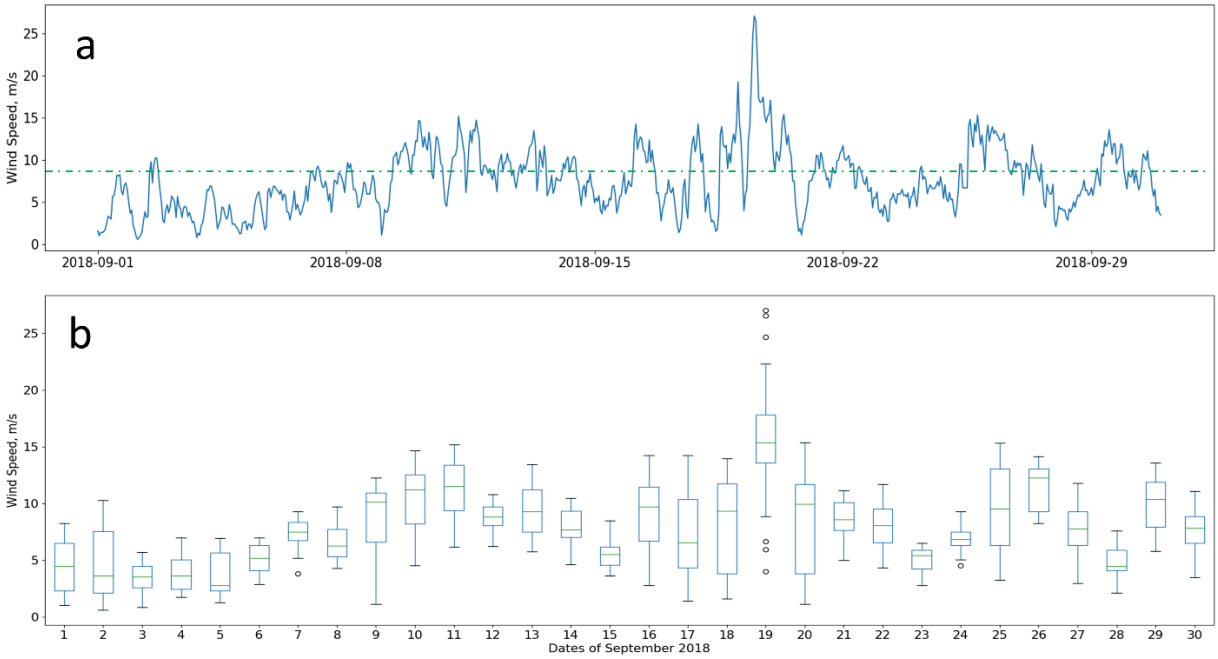

Fig. 4 – Wind speed time series visualization in line plot (a) and box plot (b).

4.2 Correlations

Time series forecasting is based on correlations between the current observation and previous observations. The correlations within the used wind speed dataset (September 2018) were explored in Fig. 5a and b, respectively. As presented in Fig. 5a, the relationship between each observation at time t and a lag of that observation at time $t-1$ is displayed through a lag plot. As can be seen, the point cluster along the diagonal line is increasing from the bottom-left to the top-right, where a strong correlation is displayed, indicating the current time series are predictable. In Fig. 5b, the strength of the correlation is quantified between wind speeds and their lags by autocorrelation, where correlation coefficients were calculated for each observation and their lag values. Autocorrelation is one of the approaches that can display correlation coefficients for a variable over successive time intervals, also known as serial correlation. The correlation coefficients were values that range between -1 and 1, where its sign represents a negative or a positive correlation, respectively. A weak correlation is represented if a correlation coefficient trends to be zero, whereas a value closes to -1 or 1 shows a strong correlation. The variations of correlation coefficients over lags are shown in Fig. 5b, at which correlation values that are above or below the dotted lines are considered as statistically significant. Both negative and positive correlations were observed in the current wind speed time series, which captures the relationship of observation with its past observations in the same and the opposite seasons. Besides, the sine-alike waves are a strong sign of seasonality.

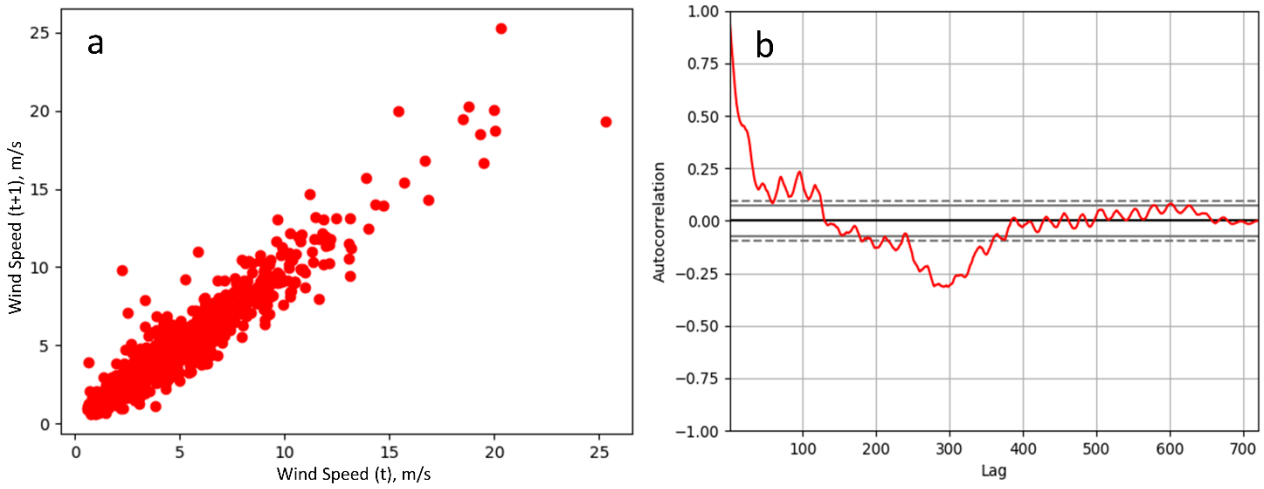

Fig. 5 – Lag plot (a) and autocorrelation (b) of wind speed time series.

4.3 Grid search

In this paper, the SARIMA model was developed to forecast offshore wind speeds in future time steps, which takes the index of time series as arguments. The one-month hourly-measured offshore wind speed time series were split into the training dataset and the testing dataset, which were recorded at the height of 110 m on September 2018. More specifically, the first 29 days of offshore wind speed measurements (01.09.2018 ~ 29.09.2018) were used for training while the last 24 h data (30.09.2018) were applied for testing.

Given that a predictive model can only be fit proficiently on modest-sized input data, grid searching is a valuable approach for hyperparameter optimization. In this study, hyperparameters in the SARIMA model were finely tuned using grid search, which automated the process of assessing predictions by different combinations of the six parameters of p, d, q, P, D, and Q. The periodicity of the time series s is set as 24 because hourly-recorded wind speed was used in this investigation. An iterative method to grid search SARIMA hyperparameters was developed for evaluating different sets of nonseasonal and seasonal lag values (p and P) in the range of 0 ~ 5, nonseasonal and seasonal difference iterations (d and D) in the range of (0 ~ 5) and nonseasonal and seasonal residual error of lag values (q and Q) in the range of (0 ~ 5). Offshore wind speed forecasting was carried out in each iteration and all predicted values were compared to met mast measurements, where a Mean Squared Error (MSE) score was recorded. The best hyperparameters of $p(2)$, $d(0)$, $q(3)$, $P(2)$, $D(1)$, $Q(3)$ are adopted in the current SARIMA model while the lowest value of MSE of 1.4292 was obtained.

4.4 Modelling results

In this study, the one-step walk-forward validation was applied during the SARIMA forecasting, where a further trained model was fitted for each rolling time intervals and tested on the next time step. Even though this process is computationally expensive, it makes certain the healthiness of the SARIMA model fitting. The rolling predicted offshore wind speeds (green

solid lines) showed a great match with the recorded values from the met mast (blue dashed lines) in Fig. 6, where both curves presented the same trend and are in the correct scale.

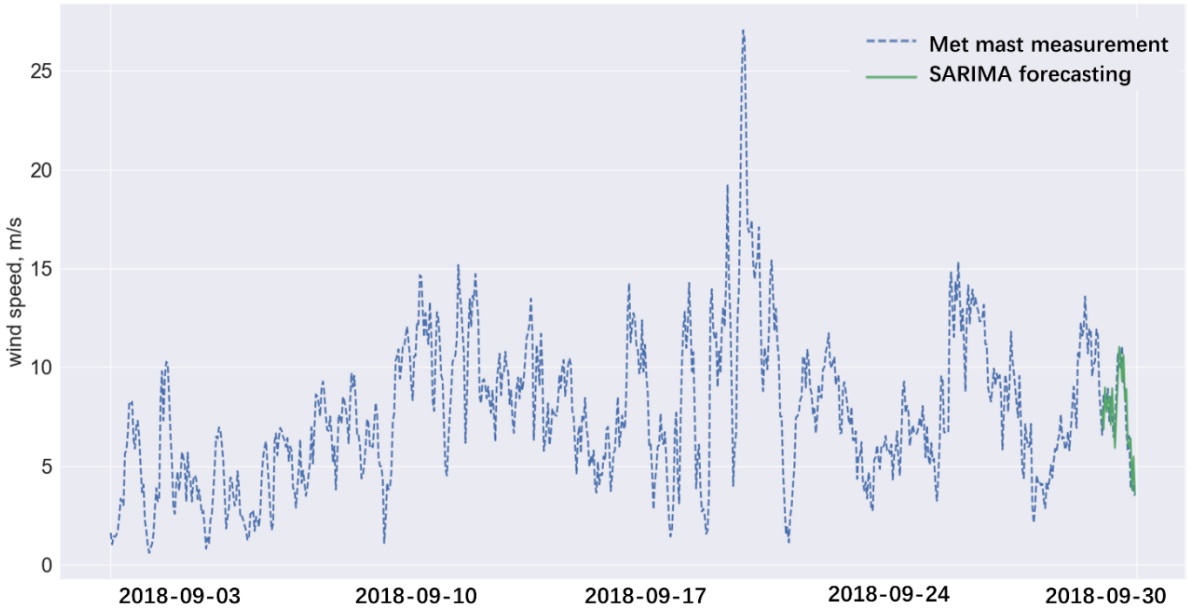

Fig. 6 – Comparisons between SARIMA rolling predictions and met mast measurements.

The differences between true and predicted offshore wind speeds (residual errors) are plotted against time intervals in Fig. 7a, indicating that most trends in time series have been captured as errors were varying around the value of zero (see the baseline of Fig. 7a). The kernel density estimation (KDE) and the histogram of standardized residuals are further displayed in Fig. 7b along with a Normal (0,1) density plot as the reference, implying the errors are Gaussian distributed and are centred near zero. In Fig. 7c, a quantile-quantile scatterplot was presented between the set of quantiles of measured offshore wind speeds and the set of quantiles of SARIMA forecasting. It proved that both sets of quantiles are normally distributed as a nearly straight line was formed. Note that, the red line was marked as a reference. Besides, in the correlogram of Fig. 7d, the autocorrelation revealed that there are almost no left correlations between residuals. Based on the sub-plots in Fig. 7, the SARIMA wind speed predictions have achieved a great agreement with the recorded met mast data and there is roughly no information remained in the residuals that can be used for further forecasting.

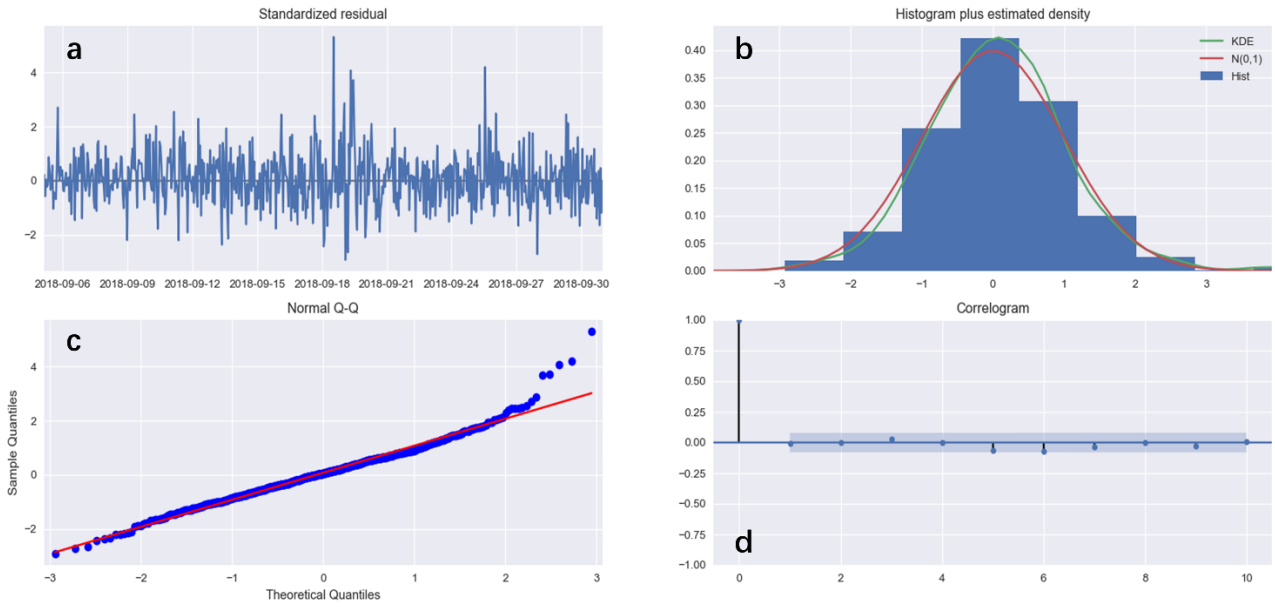

Fig. 7 – Standardized residual (a), histogram plus estimated density (b), normal quantiles-quantiles (c) and correlogram (d) of residual errors.

5. Comparisons against deep-learning-based GRU and LSTM

In this paper, deep-learning-based Gated Recurrent Neural Networks (GRNNs), in particular Long Short-Term Memory (LSTM) and Gated Recurrent Units (GRU), were introduced to compare their time series forecasting results with the ones from the developed SARIMA model. Both LSTM and GRU have the uniform goal of tracking long-term dependencies while alleviating the vanishing gradient problems that often happened in the training phase of vanilla Recurrent Neural Networks (RNNs). LSTM was initially introduced by Hochreiter and Schmidhuber [53] in 1997 and its unit consists of three gates, including a forget gate, an output gate, and an input gate. In GRU, the preliminary assembly of three gates cell from LSTM is bonded into a cell composition with only two gates (an update gate and a reset gate). GRU was subsequently proposed based on the LSTM and was regularly considered to have more compact and simpler structures. As LSTM and GRU share a similar configuration, only the details of GRU are introduced in this session, but both the performances of LSTM and GRU would be evaluated against the SARIMA-based predictive models.

5.1 GRU (Gated Recurrent Units)

GRU was firstly introduced by Cho et al. [54] in 2014 to address the vanishing gradient problem that was often suffered from standard RNNs. A typical layout of the GRU unit is presented in Fig. 8. In GRU, both the reset gate and the update gate are employed to solve the vanishing gradient problem, which are two vectors that can manipulate info in networks/layers flowing to the desired output. What makes the two gates special is that they can be trained to keep memories from long term, without removing relevant information that is significant for further predictions. In the GRU neural networks, the individual

hidden unit could be used to capture dependencies, determined by the activity frequency of the corresponding gating mechanisms. The update gate is operated to resolve how much information from previous time steps is required to be fed into future steps while the reset gate can assistant the model to determine how much past information can be forgotten [54]. Through this powerful design, GRU can take all the required info from the past and effectively reduce the hazard of vanishing gradient problem.

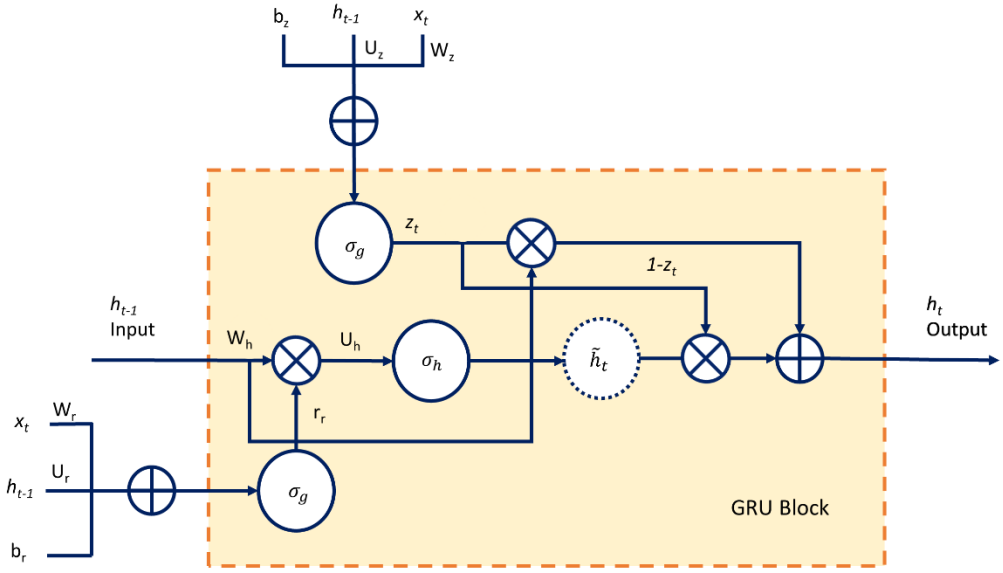

Fig. 8 – Structure of a GRU block.

The operation for the two gates could be initialized from calculating the update gate z_t for time step t through Eq. (8):

$$f_t = \sigma_g(W_z x_t + U_z h_{t-1} + b_z) \tag{8}$$

where f_t is the update gate; σ_g is the activation function; W_z and U_z are the assigned weights; x_t is the input of neuron at time step t; h_{t-1} is the cell state vector for time step $t-1$; b_z refers to the corresponding bias.

When x_t is input into a GRU unit, it will be multiplied by its corresponding weight W_z. The same happens to h_{t-1} that contains the info from the previous time step $t-1$, which will also be multiplied by its corresponding weight U_z. Then, both items are added together with the application of the activation function σ_g.

After that, the reset gate is calculated by Eq. (9):

$$r_t = \sigma_g(W_r x_t + U_r h_{t-1} + b_r) \tag{9}$$

where r_t is the reset gate; σ_g is the activation function; W_r and U_r are the assigned weights; x_t is the input of neuron at time step t; h_{t-1} is the cell state vector for time step $t-1$; b_r refers to the corresponding bias.

The equations of the update (Eq. (8)) and the reset (Eq. (9)) gates are expressed in the same form. The major differences come from the used weights and the usages of the corresponding gates. For the reset gate, it is used to select how much information from the past can be forgotten.

Then, the calculated reset gate is used to introduce a new memory content in Eq. (10)

$$\tilde{h}_t = \sigma_h(W_h x_t + (r_t \circ U_h h_{t-1}) + b_h) \tag{10}$$

where $\tilde{h}_t$ is the output candidate of the cell state vector; σ_h is the activation function; W_h and U_h are the assigned weights; x_t is the input of neuron at time step t; r_t is the reset gate; h_{t-1} is the cell state vector for time step $t-1$; b_h refers to the corresponding bias.

In Eq. (10), the Hadamard (elementwise) product is calculated between $U_h h_{t-1}$ and the reset gate r_t, which is operated to determine what information to eliminate from previous time steps. Afterwards, the activity function of σ_h is applied to produce the output candidate of the cell state vector ($\tilde{h}_t$).

Finally, the current cell state vector (h_t) is calculated to pass down the hold information to the next unit. To do so, the update gate (z_t) is involved in Eq. (11):

$$h_t = f_t \circ h_{t-1} + (1 - z_t) \circ \tilde{h}_t \tag{11}$$

where h_t is the cell state vector for time step t; f_t is the update gate; h_{t-1} is the cell state vector for time step $t-1$; $\tilde{h}_t$ is the output candidate of the cell state vector.

In Eq. (11), the elementwise multiplication is applied to both z_t & h_{t-1} and $1 - z_t$ & $\tilde{h}_t$, respectively. The two items are then summed to obtain the current cell state vector (h_t).

5.2 Model configuration

In this investigation, both GRU and LSTM shared an identical deep learning configuration, which has three input layers and one output layer. The number of neurons in the input layers were set as 50 while a single neuron was designed in the output layer. Before entering into the deep learning model, input data were transformed into a matrix with three dimensions of *batch*, *input*, and *shape*, where *batch* is the number of independent observations in the time series; *input* is the sequence length of the given observation; *shape* is the number of features at the observation time. More specifically, in the current deep learning neural networks, the used univariate sequence, which consists of hourly recorded offshore wind speed in one month, was converted into multiple samples. Each sample contains only one time step that is used to output a single future step. Besides, as univariate time series are involved, the number of features was also defined as 1 for the only variable of wind speed. When the deep learning neural networks were compiled, the MSE was specified as the loss function while the adaptive moment estimation (Adam) is applied as the optimization algorithm. Similar to other machine learning models, GRNN models can only work well

whereas the involved time series data are on the scale of a certain range. In this study, all inputs were scaled between 0 and 1 before feeding into the deep learning layers. Furthermore, the number of epochs were detected as 50 in the current predictive configuration. In this paper, the type of GRNN models, number of hidden layers, neurons in each hidden layer and number of epochs were adjusted using manual search through assessing various network configurations. Besides, following the previously designed SARIMA model, the GRNN deep learning neural networks were also validated through the walk-forward rolling prediction, indicating each time step in offshore wind speed forecasting will be rolled at a time. After the GRNN predictive model developed a prediction for one time step, the actual recorded offshore wind speed will be grasped and further used in predictions for the next time step.

5.3 Performance evaluation

To validate the reliability of the built SARIMA model, it was further compared with the forecasting results from both LSTM and GRU (see Fig. 9). In total, two different hourly-measured offshore wind speed time series (one-month span) were evaluated, which were measured at the height of 27m on April 2018 and at the height of 67m on August 2018, respectively. Again, the first 29 days of the time series (01.04.2018 ~ 29.04.2018 and 01.08.2018 ~ 29.08.2018) were used as the training datasets while the last 24 h data (30.04.2018 and 30.08.2018) were extracted as the testing datasets. As presented in Fig. 9, the SARIMA, GRU, and LSTM models displayed a great agreement with the recorded offshore wind speeds in both cases, following the same tendency of actual measurements. However, all three predictive models showed a delay along with the entire time series.

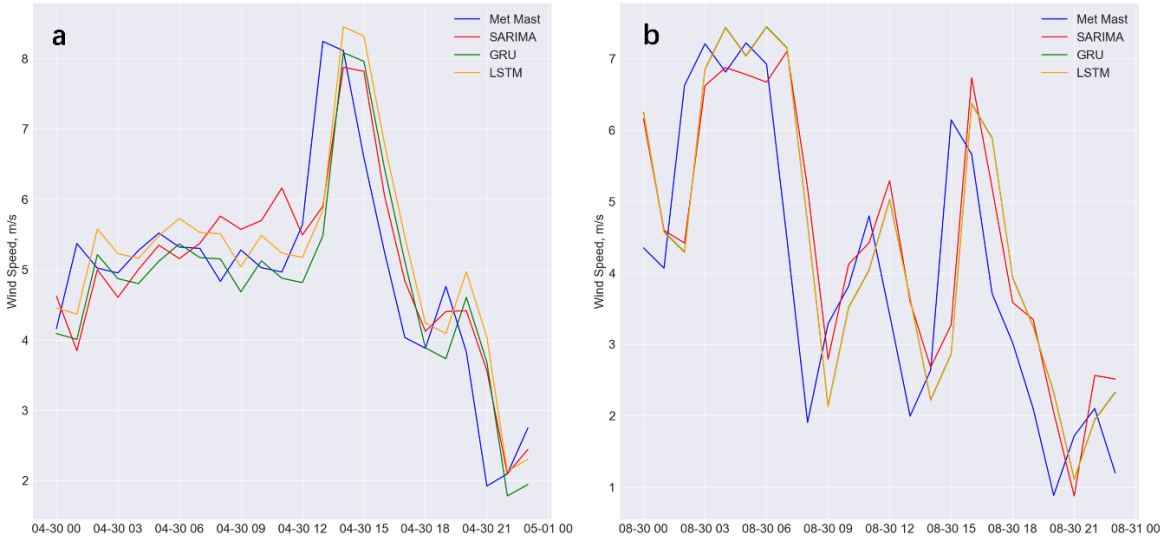

Fig. 9 – Comparison of offshore wind speed forecasting among SARIMA, GRU, LSTM and actual met mast measurements (note that, the date and time format of "MM-dd HH" is followed along the horizontal axis of **Fig.9a** and **Fig.9b**, where MM is representing months, dd is representing dates, HH is representing hours.).

When wind speed forecasting models (SARIMA, GRU, and LSTM) were compared against met mast measurements, two major mismatches were observed, including phase errors and amplitude errors (see Fig.10). Phase errors are caused by the horizontal mismatches that lag the predicted offshore wind speeds while amplitude errors define vertical deviations once the values are under/overestimated [55]. As can be seen, lagging phase errors are dominant in all the three forecasting models, since predictions are processed based on past time series. For time series forecasting, those are expected behaviours and commonly suffered phenomena because both SARIMA and GRNN operated their forecasting based on historic values of offshore wind speeds.

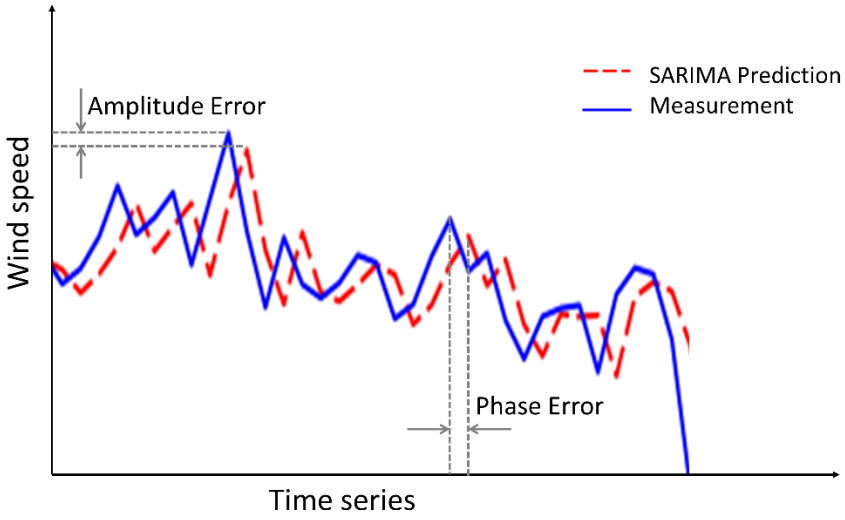

Fig. 10 – Observed errors in offshore wind speed forecasting.

To quantitatively assess the functioning of the investigated predictive models, six diverse metric measurements were further used in this study, including R-square (R^2) [56], Explained Variance Score (*EVS*) [57], Root Mean Square Error (RMSE), MSE, Mean Absolute Error (*MAE*) [58,59], and Median Absolute Error (*MedAE*) [60], which are stated in Eqs. (12), (13), (14), (15), (16), and (17), respectively:

$$R^2 = 1 - \frac{\sum_{t=1}^{n}\left[(X_{forecasting})_t - (X_{recorded})_t\right]^2}{\sum_{t=1}^{n}\left[(X_{recorded})_t - \frac{1}{n}\sum_{t=1}^{n}(X_{recorded})_t\right]^2} \tag{12}$$

$$EVS = 1 - \frac{Var\{X_{recorded} - X_{forecasting}\}}{Var\{X_{recorded}\}} \tag{13}$$

$$RMSE = \sqrt{\frac{1}{n}\sum_{t=1}^{n}\left[(X_{forecasting})_t - (X_{recorded})_t\right]^2} \tag{14}$$

$$MSE = \frac{1}{n}\sum_{t=1}^{n}\left[(X_{forecasting})_t - (X_{recorded})_t\right]^2 \quad (15)$$

$$MAE = \frac{1}{n}\sum_{t=1}^{n}\left|(X_{forecasting})_t - (X_{recorded})_t\right| \quad (16)$$

$$MedAE = median\left(\left|(X_{forecasting})_1 - (X_{recorded})_1\right|, \ldots, \left|(X_{forecasting})_t - (X_{recorded})_t\right|\right) \quad (17)$$

where $(X_{recorded})_t$ is the recorded offshore wind speed at the time step t, $(X_{forecasting})_t$ is the predicted offshore wind speed at the identical time step; n is the number of time steps.

The forecasting performance of SARIMA, GRU and LSTM were further compared in Table 2 by the proposed six metric functions, determining the level of accuracy of those predictive models. For R^2 and EVS, both offer measures of how far actual observations differ from the forecasted values. The higher the R^2 or EVS score is, the more accurate the predictive models are. Both R^2 and EVS scores are in the range of 0.0 ~ 1.0, where the best possible value is 1.0 and lower scores are worse. Besides, if negative values of R^2 or EVS were observed, it indicates that the corresponding predictive model has become arbitrarily worse. Conversely to R^2 and EVS, notwithstanding RMSE, MSE, MAE, and MedAE are also used to evaluate the discrepancy between the actual data and the predictive models, their low values are representing a high level of accuracy and a better prediction. As presented in Table 2, relatively high accuracies were achieved in all three cases. However, it can also be observed that greater values of R2/EVS and lower values of RMSE/MSE/MAE/MedAE were gained in the case of SARIMA models in all time series cases on April, August, and September 2018, indicating, in general, the proposed SARIMA model provided a better performance compared with GRU and LSTM.

In time series forecasting, deep-learning-based algorithms often require more historical data to train and more hyperparameters to tune than other models. The occurred underperformances of GRU and LSTM could be caused by overfitting. This phenomenon often takes place when the used machine learning algorithm matches well in the training process while the predicting model has a difficult time to be specified in testing or validation datasets. In this study, relatively small time-series datasets (one-month span) were used for training predictive models, where both GRU and LSTM are more likely to overlook existing patterns within seasonal periods. This could further result in higher variance and higher errors in the deep-learning-based algorithms.

Table 2 – Performance of SARIMA, GRU and LSTM models under different metric functions in wind speed forecasting.

	Predictive models	*R2*	*EVS*	*RMSE*	*MSE*	*MAE*	*MedAE*
Case 1 (25m)	SARIMA	0.6619	0.6695	0.8486	0.7201	0.6168	0.3521
	GRU	0.5884	0.5920	0.9364	0.8768	0.6578	0.4351
	LSTM	0.5587	0.5931	0.9695	0.9400	0.7175	0.4510

Case 2 (67m)	SARIMA	0.4626	0.5196	1.4553	2.1178	1.1469	0.9559
	GRU	0.4235	0.4700	1.5073	2.2720	1.2232	1.0209
	LSTM	0.4255	0.4700	1.5047	2.2641	1.2216	1.0115
Case 3 (110 m)	SARIMA	0.5411	0.5465	1.4292	2.0427	1.2489	1.1513
	GRU	0.5120	0.5281	1.4739	2.1722	1.2494	1.2139
	LSTM	0.5320	0.5334	1.4446	2.0868	1.2491	1.1628

6. Conclusions

In this paper, SARIMA forecasting models were evaluated based on wind speed time series measured at three different heights from a coastal met mast in Scotland. The SARIMA models were accomplished in several steps defined by the adopted approaches, which involved resampling the raw data to ensure high-quality datasets, identifying temporal structures of trend and seasonality in the time series, and analysing residual errors to make sure no information remained in the used data. The proposed SARIMA models were further compared against the deep-learning-based GRNN models (both GRU and LSTM) through six different metric functions. To maximize performances, both SARIMA models and GRNN deep learning models were hyperparameter tuned via a combination of manual and grid search. Based on the modelling performances on difference offshore wind speed time series measured at various elevations, the SARIMA approach outperformed the deep learning-based algorithms of both GRU and LSTM.

It is more suitable to address offshore wind speed by the SARIMA approach, which directly supports the forecasts of seasonal components in univariate datasets. Furthermore, the SARIMA model only requires to turn the six parameters of (p, q, d, P, Q, D) while more hyperparameters need to be evaluated in GRU or LSTM, such as number of units in each layer, number of layers, batch size, number of epochs, optimizer, activation function, kernel initializer, and so forth. Even though accurate offshore wind speed predictions have received much attention in recent decades, conventional neural networks do not appear to be effective enough at addressing short-term time sequences. Some machine learning predictive models can easily fall into over-fitting or local optimum. The SARIMA approach can be more straightforward and more efficient tool than deep-learning-based GRNN models in forecasting offshore wind speed time series.

Acknowledgement

The authors thank the Offshore Renewable Energy (ORE) Catapult for provisions of the met mast database.

References

[1] IRENA. Future of wind: Deployment, investment, technology, grid integration and socio-economic aspects (A Global Energy Transformation paper), International Renewable Energy Agency. Abu Dhabi: 2019.

[2] Lin Z, Liu X, Collu M. Wind power prediction based on high-frequency SCADA data along with isolation forest and deep learning neural networks. International Journal of Electrical Power and Energy Systems 2020;118:105835. https://doi.org/10.1016/j.ijepes.2020.105835.
[3] Lin Z, Liu X. Assessment of wind turbine aero-hydro-servo-elastic modelling on the effects of mooring line tension via deep learning. Energies 2020;13:2264.
[4] Aasim, Singh SN, Mohapatra A. Repeated wavelet transform based ARIMA model for very short-term wind speed forecasting. Renewable Energy 2019;136:758–68. https://doi.org/https://doi.org/10.1016/j.renene.2019.01.031.
[5] Hanifi S, Liu X, Lin Z, Lotfian S. A Critical Review of Wind Power Forecasting Methods—Past, Present and Future. Energies 2020;13:3764. https://doi.org/10.3390/en13153764.
[6] Hu J, Wang J, Ma K. A hybrid technique for short-term wind speed prediction. Energy 2015;81:563–74. https://doi.org/10.1016/j.energy.2014.12.074.
[7] Troncoso A, Salcedo-Sanz S, Casanova-Mateo C, Riquelme JC, Prieto L. Local models-based regression trees for very short-term wind speed prediction. Renewable Energy 2015;81:589–98. https://doi.org/10.1016/j.renene.2015.03.071.
[8] Ramasamy P, Chandel SS, Yadav AK. Wind speed prediction in the mountainous region of India using an artificial neural network model. Renewable Energy 2015;80:338–47. https://doi.org/https://doi.org/10.1016/j.renene.2015.02.034.
[9] Liu H, Tian H, Liang X, Li Y. Wind speed forecasting approach using secondary decomposition algorithm and Elman neural networks. Applied Energy 2015;157:183–94. https://doi.org/https://doi.org/10.1016/j.apenergy.2015.08.014.
[10] Fei S, He Y. Wind speed prediction using the hybrid model of wavelet decomposition and artificial bee colony algorithm-based relevance vector machine. International Journal of Electrical Power & Energy Systems 2015;73:625–31. https://doi.org/https://doi.org/10.1016/j.ijepes.2015.04.019.
[11] Zhang C, Wei H, Zhao X, Liu T, Zhang K. A Gaussian process regression based hybrid approach for short-term wind speed prediction. Energy Conversion and Management 2016;126:1084–92. https://doi.org/https://doi.org/10.1016/j.enconman.2016.08.086.
[12] Santamaría-Bonfil G, Reyes-Ballesteros A, Gershenson C. Wind speed forecasting for wind farms: A method based on support vector regression. Renewable Energy 2016;85:790–809. https://doi.org/https://doi.org/10.1016/j.renene.2015.07.004.
[13] Shrivastava NA, Lohia K, Panigrahi BK. A multiobjective framework for wind speed prediction interval forecasts. Renewable Energy 2016;87:903–10. https://doi.org/https://doi.org/10.1016/j.renene.2015.08.038.
[14] Sun W, Liu M. Wind speed forecasting using FEEMD echo state networks with RELM in Hebei, China. Energy Conversion and Management 2016;114:197–208. https://doi.org/https://doi.org/10.1016/j.enconman.2016.02.022.
[15] Meng A, Ge J, Yin H, Chen S. Wind speed forecasting based on wavelet packet decomposition and artificial neural networks trained by crisscross optimization algorithm. Energy Conversion and Management 2016;114:75–88. https://doi.org/10.1016/j.enconman.2016.02.013.
[16] Lydia M, Suresh Kumar S, Immanuel Selvakumar A, Edwin Prem Kumar G. Linear and non-linear autoregressive models for short-term wind speed forecasting. Energy Conversion and Management 2016;112:115–24. https://doi.org/https://doi.org/10.1016/j.enconman.2016.01.007.
[17] Fazelpour F, Tarashkar N, Rosen MA. Short-term wind speed forecasting using artificial neural networks for Tehran, Iran. International Journal of Energy and Environmental Engineering 2016;7:377–90. https://doi.org/10.1007/s40095-016-0220-6.
[18] Doucoure B, Agbossou K, Cardenas A. Time series prediction using artificial wavelet neural network and multi-resolution analysis: Application to wind speed data. Renewable Energy 2016;92:202–11. https://doi.org/https://doi.org/10.1016/j.renene.2016.02.003.
[19] Jiang Y, Huang G. Short-term wind speed prediction: Hybrid of ensemble empirical mode decomposition, feature selection and error correction. Energy Conversion and Management 2017;144:340–50. https://doi.org/https://doi.org/10.1016/j.enconman.2017.04.064.
[20] Ambach D, Schmid W. A new high-dimensional time series approach for wind speed, wind direction and air pressure forecasting. Energy 2017;135:833–50. https://doi.org/https://doi.org/10.1016/j.energy.2017.06.137.
[21] Han Q, Meng F, Hu T, Chu F. Non-parametric hybrid models for wind speed forecasting. Energy Conversion and Management 2017;148:554–68. https://doi.org/https://doi.org/10.1016/j.enconman.2017.06.021.
[22] Yu C, Li Y, Zhang M. An improved Wavelet Transform using Singular Spectrum Analysis for wind speed forecasting based on Elman Neural Network. Energy Conversion and Management 2017;148:895–904. https://doi.org/10.1016/j.enconman.2017.05.063.
[23] Ma X, Jin Y, Dong Q. A generalized dynamic fuzzy neural network based on singular spectrum analysis optimized by brain storm optimization for short-term wind speed forecasting. Applied Soft Computing 2017;54:296–312. https://doi.org/https://doi.org/10.1016/j.asoc.2017.01.033.

[24] Yu C, Li Y, Zhang M. Comparative study on three new hybrid models using Elman Neural Network and Empirical Mode Decomposition based technologies improved by Singular Spectrum Analysis for hour-ahead wind speed forecasting. Energy Conversion and Management 2017;147:75–85. https://doi.org/10.1016/j.enconman.2017.05.008.
[25] Chang GW, Lu HJ, Chang YR, Lee YD. An improved neural network-based approach for short-term wind speed and power forecast. Renewable Energy 2017;105:301–11. https://doi.org/https://doi.org/10.1016/j.renene.2016.12.071.
[26] Chen J, Zeng G-Q, Zhou W, Du W, Lu K-D. Wind speed forecasting using nonlinear-learning ensemble of deep learning time series prediction and extremal optimization. Energy Conversion and Management 2018;165:681–95. https://doi.org/https://doi.org/10.1016/j.enconman.2018.03.098.
[27] Wang L, Li X, Bai Y. Short-term wind speed prediction using an extreme learning machine model with error correction. Energy Conversion and Management 2018;162:239–50. https://doi.org/https://doi.org/10.1016/j.enconman.2018.02.015.
[28] Naik J, Satapathy P, Dash PK. Short-term wind speed and wind power prediction using hybrid empirical mode decomposition and kernel ridge regression. Applied Soft Computing 2018;70:1167–88. https://doi.org/https://doi.org/10.1016/j.asoc.2017.12.010.
[29] Li C, Xiao Z, Xia X, Zou W, Zhang C. A hybrid model based on synchronous optimisation for multi-step short-term wind speed forecasting. Applied Energy 2018;215:131–44. https://doi.org/https://doi.org/10.1016/j.apenergy.2018.01.094.
[30] Deo RC, Ghorbani MA, Samadianfard S, Maraseni T, Bilgili M, Biazar M. Multi-layer perceptron hybrid model integrated with the firefly optimizer algorithm for windspeed prediction of target site using a limited set of neighboring reference station data. Renewable Energy 2018;116:309–23. https://doi.org/https://doi.org/10.1016/j.renene.2017.09.078.
[31] Khosravi A, Machado L, Nunes RO. Time-series prediction of wind speed using machine learning algorithms: A case study Osorio wind farm, Brazil. Applied Energy 2018;224:550–66. https://doi.org/10.1016/j.apenergy.2018.05.043.
[32] Li Y, Shi H, Han F, Duan Z, Liu H. Smart wind speed forecasting approach using various boosting algorithms, big multi-step forecasting strategy. Renewable Energy 2019;135:540–53. https://doi.org/https://doi.org/10.1016/j.renene.2018.12.035.
[33] Fu W, Wang K, Li C, Tan J. Multi-step short-term wind speed forecasting approach based on multi-scale dominant ingredient chaotic analysis, improved hybrid GWO-SCA optimization and ELM. Energy Conversion and Management 2019;187:356–77. https://doi.org/https://doi.org/10.1016/j.enconman.2019.02.086.
[34] García I, Huo S, Prado R, Bravo L. Dynamic bayesian temporal modeling and forecasting of short-term wind measurements. Renewable Energy 2020. https://doi.org/https://doi.org/10.1016/j.renene.2020.05.182.
[35] Zhang Y, Pan G, Chen B, Han J, Zhao Y, Zhang C. Short-term wind speed prediction model based on GA-ANN improved by VMD. Renewable Energy 2019. https://doi.org/10.1016/j.renene.2019.12.047.
[36] Wei C. Development of Stacked Long Short-Term Memory Neural Networks with Numerical Solutions for Wind Velocity Predictions. Advances in Meteorology 2020;2020.
[37] Schiermeier Q. And now for the energy forecast: Germany works to predict wind and solar power generation. Nature 2016;535.
[38] Wang X, Guo P, Huang X. A review of wind power forecasting models. Energy Procedia, vol. 12, Elsevier Ltd; 2011, p. 770–8. https://doi.org/10.1016/j.egypro.2011.10.103.
[39] Kavasseri RG, Seetharaman K. Day-ahead wind speed forecasting using f-ARIMA models. Renewable Energy 2009;34:1388–93. https://doi.org/https://doi.org/10.1016/j.renene.2008.09.006.
[40] Cadenas E, Rivera W. Wind speed forecasting in three different regions of Mexico, using a hybrid ARIMA–ANN model. Renewable Energy 2010;35:2732–8. https://doi.org/https://doi.org/10.1016/j.renene.2010.04.022.
[41] Shukur OB, Lee MH. Daily wind speed forecasting through hybrid KF-ANN model based on ARIMA. Renewable Energy 2015;76:637–47. https://doi.org/https://doi.org/10.1016/j.renene.2014.11.084.
[42] Wang J, Hu J. A robust combination approach for short-term wind speed forecasting and analysis – Combination of the ARIMA (Autoregressive Integrated Moving Average), ELM (Extreme Learning Machine), SVM (Support Vector Machine) and LSSVM (Least Square SVM) forecasts usi. Energy 2015;93:41–56. https://doi.org/https://doi.org/10.1016/j.energy.2015.08.045.
[43] Eymen A, Köylü Ü. Seasonal trend analysis and ARIMA modeling of relative humidity and wind speed time series around Yamula Dam. Meteorology and Atmospheric Physics 2019;131:601–12. https://doi.org/10.1007/s00703-018-0591-8.
[44] Fang T, Lahdelma R. Evaluation of a multiple linear regression model and SARIMA model in forecasting heat demand for district heating system. Applied Energy 2016;179:544–52. https://doi.org/https://doi.org/10.1016/j.apenergy.2016.06.133.
[45] Kushwaha V, Pindoriya NM. A SARIMA-RVFL hybrid model assisted by wavelet decomposition for very short-term solar PV power generation forecast. Renewable Energy 2019;140:124–39. https://doi.org/https://doi.org/10.1016/j.renene.2019.03.020.

[46] Guo Z, Zhao J, Zhang W, Wang J. A corrected hybrid approach for wind speed prediction in Hexi Corridor of China. Energy 2011;36:1668–79. https://doi.org/10.1016/j.energy.2010.12.063.
[47] Lin Z, Liu X, Lao L, Liu H. Prediction of two-phase flow patterns in upward inclined pipes via deep learning. Energy 2020;210:118541. https://doi.org/10.1016/j.energy.2020.118541.
[48] Kisvari A, Lin Z, Liu X. Wind power forecasting – A data-driven method along with gated recurrent neural network. Renewable Energy 2021;163:1895–909. https://doi.org/10.1016/j.renene.2020.10.119.
[49] Lin Z, Liu X. Wind power forecasting of an offshore wind turbine based on high-frequency SCADA data and deep learning neural network. Energy 2020. https://doi.org/https://doi.org/10.1016/j.energy.2020.117693.
[50] ORE Catapult. LDT Met Mast SCADA-1sec | POD 2020. https://pod.ore.catapult.org.uk/data-collection/ldt-met-mast-scada-1sec (accessed December 21, 2020).
[51] Yamak PT, Yujian L, Gadosey PK. A Comparison between ARIMA, LSTM, and GRU for Time Series Forecasting. Proceedings of the 2019 2nd International Conference on Algorithms, Computing and Artificial Intelligence, 2019, p. 49–55.
[52] Box GEP, Jenkins GM, Reinsel GC, Ljung GM. Time series analysis: forecasting and control. John Wiley & Sons; 2015.
[53] Hochreiter S, Schmidhuber J. Long Short-Term Memory. Neural Computation 1997;9. https://doi.org/https://doi.org/10.1162/neco.1997.9.8.1735.
[54] Cho K, Van Merriënboer B, Gulcehre C, Bahdanau D, Bougares F, Schwenk H, et al. Learning phrase representations using RNN encoder-decoder for statistical machine translation. EMNLP 2014 - 2014 Conference on Empirical Methods in Natural Language Processing, Proceedings of the Conference 2014:1724–34. https://doi.org/10.3115/v1/d14-1179.
[55] Xu M, Qiao Y, Lu Z, others. A comprehensive error evaluation method for short-term wind power prediction. Dianli Xitong Zidonghua(Automation of Electric Power Systems) 2011;35:20–6.
[56] Mashaly AF, Alazba AA, Al-Awaadh AM, Mattar MA. Predictive model for assessing and optimizing solar still performance using artificial neural network under hyper arid environment. Solar Energy 2015;118:41–58. https://doi.org/10.1016/j.solener.2015.05.013.
[57] Huijbregts MAJ, Rombouts LJA, Hellweg S, Frischknecht R, Hendriks AJ, Van De Meent D, et al. Is cumulative fossil energy demand a useful indicator for the environmental performance of products? Environmental Science and Technology 2006;40:641–8. https://doi.org/10.1021/es051689g.
[58] Zhao Y, Ye L, Pinson P, Tang Y, Lu P. Correlation-Constrained and Sparsity-Controlled Vector Autoregressive Model for Spatio-Temporal Wind Power Forecasting. IEEE Transactions on Power Systems 2018;33:5029–40. https://doi.org/10.1109/TPWRS.2018.2794450.
[59] Chen N, Qian Z, Nabney IT, Meng X. Wind power forecasts using gaussian processes and numerical weather prediction. IEEE Transactions on Power Systems 2014;29:656–65. https://doi.org/10.1109/TPWRS.2013.2282366.
[60] Saad E, Shammas MC, Shammas HJ. Scheimpflug Corneal Power Measurements for Intraocular Lens Power Calculation in Cataract Surgery. American Journal of Ophthalmology 2013;156:460-467.e2. https://doi.org/https://doi.org/10.1016/j.ajo.2013.04.035.